Khoramgah et al., *BioImpacts,* 2023, 13(1), 31-42
doi: 10.34172/bi.2021.23711
http://bi.tbzmed.ac.ir/

Repairing rat calvarial defects by adipose mesenchymal stem cells and novel freeze-dried three-dimensional nanofibrous scaffolds

Maryam Sadat Khoramgah[1,2,3,4], Hossein Ghanbarian[1,4], Javad Ranjbari[1,4], Nilufar Ebrahimi[3,5], Fatemeh Sadat Tabatabaei Mirakabad[1,4], Navid Ahmady Roozbahany[3,6], Hojjat-Allah Abbaszadeh[2,3,7*], Simzar Hosseinzadeh[8,9*]

[1]Department of Medical Biotechnology, School of Advanced Technologies in Medicine, Shahid Beheshti University of Medical Sciences, Tehran, Iran
[2]Laser Application in Medical Sciences Research Center, Shahid Beheshti University of Medical Sciences, Tehran, Iran
[3]Hearing Disorders Research Center, Loghman Hakim Hospital, Shahid Beheshti University of Medical Sciences, Tehran, Iran
[4]Cellular and Molecular Biology Research Center, Shahid Beheshti University of Medical Sciences, Tehran, Iran
[5]Department of Biomedical Engineering, East Tehran Branch, Islamic Azad University, Tehran, Iran
[6]Private Practice, Bradford ON, Canada
[7]Department of Biology and Anatomical Sciences, School of Medicine, Shahid Beheshti University of Medical Sciences, Tehran, Iran
[8]Medical Nanotechnology and Tissue Engineering Research Center, Shahid Beheshti University of Medical Sciences, Tehran, Iran
[9]Department of Tissue Engineering and Applied Cell Sciences, School of Advanced Technologies in Medicine, Shahid Beheshti University of Medical Sciences, Tehran, Iran

Article Info

Article Type:
Original Article

Article History:
Received: 3 Mar. 2021
Revised: 14 July 2021
Accepted: 24 July 2021
ePublished: 15 Dec. 2021

Keywords:
Calvarial defect, Three dimensional nanofibrous scaffold, Polyvinyl alcohol, Polytetrafluoroethylene, Graphene oxide nanoparticle, Human adipose mesenchymal stem cells

Abstract

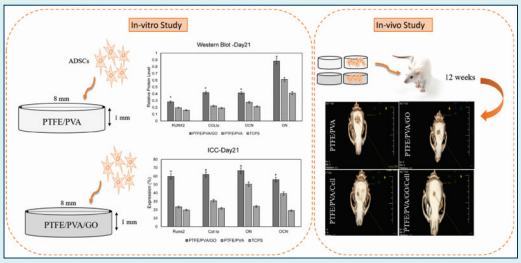

Introduction: Treatment of critical-sized bone defects is challenging. Tissue engineering as a state-of-the-art method has been concerned with treating these non-self-healing bone defects. Here, we studied the potentials of new three-dimensional nanofibrous scaffolds (3DNS) with and without human adipose mesenchymal stem cells (ADSCs) for reconstructing rat critical-sized calvarial defects (CSCD).

Methods: Scaffolds were made from 1- polytetrafluoroethylene (PTFE), and polyvinyl alcohol (PVA) (PTFE/ PVA group), and 2- PTFE, PVA, and graphene oxide (GO) nanoparticle (PTFE/ PVA/GO group) and seeded by ADSCs and incubated in osteogenic media (OM). The expression of key osteogenic proteins including Runt-related transcription factor 2 (Runx2), collagen type Iα (COL Iα), osteocalcin (OCN), and osteonectin (ON) at days 14 and 21 of culture were evaluated by western blot and immunocytochemistry methods. Next, 40 selected rats were assigned to five groups (n=8) to create CSCD which will be filled by scaffolds or cell-containing scaffolds. The groups were denominated as the following order: Control (empty defects), PTFE/PVA (PTFE/PVA scaffolds implant), PTFE/PVA/GO (PTFE/PVA/GO scaffolds implant), PTFE/PVA/Cell group (PTFE/PVA scaffolds containing ADSCs implant), and PTFE/PVA/GO/Cell group (PTFE/PVA/GO scaffolds containing ADSCs implant). Six and 12 weeks after implantation, the animals were sacrificed and bone regeneration was evaluated using computerized tomography (CT), and hematoxylin-eosin (H&E) staining.

Results: Based on the in-vitro study, expression of bone-related proteins in ADSCs seeded on PTFE/PVA/GO scaffolds were significantly higher than PTFE/PVA scaffolds and TCPS (P<0.05). Based on the in-vivo study, bone regeneration in CSCD were filled with PTFE/PVA/GO scaffolds containing ADSCs were significantly higher than PTFE/PVA scaffolds containing ADSCs (P<0.05). CSCD filled with cell-seeded scaffolds showed higher bone regeneration in comparison with CSCD filled with scaffolds only (P<0.05).

Conclusion: The data provided evidence showing new freeze-dried nanofibrous scaffolds formed from hydrophobic (PTFE) and hydrophilic (PVA) polymers with and without GO provide a suitable environment for ADSCs due to the expression of bone-related proteins. ADSCs and GO in the implanted scaffolds had a distinct effect on the bone regeneration process in this in-vivo study.

*Corresponding authors: Hojjat-Allah Abbaszadeh, Email: dr.abbaszadeh@sbmu.ac.ir; Simzar Hosseinzadeh, Email: S.hosseinzadeh@sbmu.ac.ir

Introduction

Critical-size bone defects which are non-self-healing lesions are caused by trauma, cancer, postmenopausal osteoporosis, congenital deformity, and metabolic diseases.[1,2] Current therapeutic methods such as metal implants, autografts, and allografts require multiple surgeries. They have a limited supply and may lead to an immunological response. The bone tissue engineering (BTE) approach is a promising alternative.[2,3] The success of the tissue engineering approach depends on applying the three major elements; 3D bio-scaffolds, stem cells, and tissue regeneration factors.[4]

Design and fabrication of a 3D scaffold as a temporary carrier and supporter of cells and tissue regeneration factors is a very important step in BTE.[4-6] Bone tissue scaffolds should mimic the hierarchical structures of natural bone extracellular matrix (ECM) ranging from the millimeter to the nanometer scale with suitable porosity and mechanobiology.[7,8] Micro and nanotopographical features of scaffolds have a tremendous impact on enhancing the cell attachment, proliferation, migration, and differentiate.[9-12] Besides scaffold morphology and topography, the type of scaffold biomaterials and their properties play an important role in cell-scaffold interactions[7].

Hydrogels are one of the most attractive types of biomaterial to fabricate 3D scaffolds[13] because of their soft three-dimensional network structure with high capacity of absorbing water similar to natural ECM.[4,14] Hydrogels provide a suitable surface for cell attachment that is vital to other cellular behaviors like migration and differentiation.[15] However, 3D hydrogel as a scaffold for hard tissue engineering exhibits poor mechanical properties because of the amount of water in its structure.[16] Researchers have been focused to finding a way to solve this complex scientific area in the best manner. There are many established kinds of methods to improve the mechanical properties of hydrogels such as copolymerization, incorporation, interpenetrating polymer networks, hydrophobic association hydrogels, and nanocomposites.[17,18]

Among the above-mentioned approaches, taking the advantage of hydrophobic sequence and biomaterial to make hydrophobic interaction in forming hydrogel have been considered for tissue scaffolds because of the hydrophobic-hydrophilic composite face of natural ECM. Studies showed that hydrophobic amino acids and domains in two abundant fibrous proteins in human ECM organization, collagen, and elastin have a determining effect on cell behavioral[19-21] and structural properties of ECM.[22-24]

Several studies focused on different hydrophobic polymers and nanoparticles for modifying the structural properties of hydrogels.[18] Recently we have made new 3D scaffolds by the incorporation of PTFE as a hydrophobic polymer, and polyvinyl alcohol (PVA) as a hydrophilic polymer with and without graphene oxide (GO) as an osteoinductive nanoparticle.[22] Randomly discontinued nanofibers in the range of 2-600 nm diameter were expanded in both 3D scaffolds were fabricated by freeze-drying methods under defined circumstances. Moreover, both scaffolds (PTFE/PVA and PTFE/PVA/GO) have shown multi-scale pore architecture with suitable porosity, hydrophilicity, cell attachment, and osteo-differentiation, as well as tuned mechanical and thermal properties.[22]

This study aimed to evaluate the potential of 3D nanofibrous scaffolds in the in-vivo study and to compare the effect of GO nanoparticles on in-vitro key osteogenic proteins expression by seeded human adipose mesenchymal stem cells (ADSCs). We also evaluated the regeneration of critical-sized calvarial defects (CSCD) at rat model when implanted by cell-free and cell-containing scaffolds.

Materials and Methods

Scaffolds preparation

Multiscale porous nanofibrous discoid scaffolds were made from ternary composition PVA (16% w.t solution, Mw 85 000-124 000, 99+% hydrolyzed), PTFE (CAS Number 9002-84-0), with and without synthesized GO nanoparticles (Sigma-Aldrich, Germany) in the following steps: mixing and stirring PTFE/PVA solutions (78:22) at 80°C for about 2 hours, adding 0.005 g of GO nanoparticles (only in GO incorporating groups) and sonicating for 30 minutes, crosslinking by 1 µL/mL boric acid (4%), and freeze-drying -40°C for 18 hours at Christ GAMMA 1-16 LSC Freeze Dryers. Finally, two types of cylinder-shaped (0.8 mm diameter, 2 mm height) 3D scaffold (PTEFE/PVA and PTFE/PVA/GO) were obtained.[22]

Stem cells isolation and characterization

Adipose tissues of healthy women (n=3, 36 ± 12 years old) were obtained through abdominoplasty under the support of Shahid Beheshti University's Medical Research Ethics Committee, Tehran, Iran. ADSCs were extracted enzymatically from the adipose tissues and were cultured in the following way: washing with PBS, dissecting, digesting by collagenase type I (0.075%, Sigma-Aldrich), inactivating the enzymes by Dulbecco's modified Eagle's medium (DMEM, high glucose, Gibco) with 10% fetal bovine serum (Gibco), centrifuging at 500 g × 4 minutes, collecting cell pellets, culturing in growth medium containing DMEM, 10% fetal bovine serum, and streptomycin/ penicillin (1% antibiotic, Gibco) for 24 hours at 37°C, 5% CO2. Every 2 days, the cells medium was refreshed until the 70-80% cell confluency was obtained. The isolated cell's multi linage differentiation potential was confirmed by adipose- and osteogenic differentiation assays using respectively Oil Red O and Alizarin Red Stain. Mesenchymal cell surface markers (CD) including CD14, CD20, CD34, CD45, CD73, CD90, and CD105 (Chemicon)[25] were investigated by flow cytometry (Partec

CyFlow Space cytometer). For this purpose, cells at passage 3 were collected with Trypsin/EDTA (Gibco), fixed in ice-cold formaldehyde (2%, Gibco), washed with PBS (Sigma-Aldrich), incubated at 4°C with above-mentioned antibodies conjugated with peridinin chlorophyll protein complex (PerCP), allophycocyanin (APC), fluorescein isothiocyanate (FITC), and phycoerythrin (PE) for 30 minutes, and analyzed by FlowJo V10 software. Isotype control was used for all the experiments.

Cell seeding and characterization

In summary, cultured ADSCs were detached using Trypsin-EDTA, counted by hemocytometer, transferred (4× 10^6 cells) into 50 ml centrifuge tube, centrifuged (5×g for 5 minutes), and resuspended in DMEM-F12 containing 10% FBS. Then, the scaffolds were sterilized (ethanol 70%, UV), were seeded by ADSCs (4 × 10^6/1 µL), and incubated in osteogenic differentiation media (Bioidea, Iran) containing DMEM-F12, 10% FBS, antibiotic solution, 100 nM dexamethasone, 10 mM b-glycerophosphate, and 0.2 mM ascorbic acid 2-phosphate for 14 or 21 days (in defining study's time points) at 37°C and 5% CO2. For in-vitro analysis, ADSCs seeded on tissue culture polystyrene (TCPS) were used as a control, and all procedures were done in triplicate samples. To characterize the seeded cells, one scaffold was selected randomly and underwent imaging by scanning electron and fluorescent microscope.[22]

Western blot

For evaluating the key osteogenic proteins (Runx2, Col1α, ON and OCN) expressed by seeded cells within 14 and 21 days of culture under OM, western blot was done on samples of three individual groups; PTFE/PVA/Cell, PTEFE/PVA/GO/cell, and TCPS. The steps were as follows[26,27]: washing samples with cold PBS buffer, extracting the proteins using ice-cold radio-immunoprecipitation assay buffer (Cytomatingene) containing protease inhibitor cocktail (Sigma), counting the proteins using BCA protein assay kit (Sigma), separating the proteins (30 µg for each group) on 10% SDS-polyacrylamide gels, transferring the separated proteins into PVDF membrane (Roth), blocking nonspecific sites of membrane by tris-buffered saline containing tween and 5% nonfat milk (Sigma), incubating the membrane with primary antibodies Runx2, Col1α, ON and OCN (Santa Cruz Biotechnology, 1:1000 dilution) at 4°C overnight, washing the membrane extensively with PBS-Tween, incubating the membrane with corresponding secondary HRP-conjugated antibodies (1:5000) for 1 hour at room temperature, washing membrane with PBS, developing the membrane using DAB (3, 3'-diaminobenzidine) substrate, capturing the image of blot, and semi-quantifying the image blots using ImageJ software. For normalizing the results, glyceraldehyde 3-phosphate dehydrogenase was used as a housekeeping protein.

Immunocytochemistry

To confirm the expression of above mentioned key osteogenic proteins, immunocytochemistry method[28,29] was used on day 14 and 21 of culture under OM according to the following steps: fixing the samples using 4% phosphate-buffered paraformaldehyde, embedding in paraffin, sectioning into 5 µm thickness slices, selecting appropriate samples randomly, de-waxing in xylenes, rehydrating in ethanol baths, washing twice with PBS, immersing in 0.1% Triton X-100, washing extensively with PBS, incubating with primary antibodies (Runx2, ColIα1, ON, OCN, Santa Cruz Biotechnology) at 4°C, washing samples with PBS, and incubating with fluorescence-conjugated secondary anti-mouse IgG (Santa Cruz Biotechnology) for 1 h at 37°C. Eventually, after nuclear staining with DAPI (40, 6-diamidino-2-phenylindole, Sigma), samples were imaged using a fluorescent microscope (Leica DMI 6000/NIKON).

Experimental groups and surgical procedure

To evaluate the bone regeneration potential of scaffolds and cell-containing scaffolds, forty healthy male Sprague Dawley rats (60 days old, 250-300-g weight) were provided by Pasture Institute (Tehran, Iran). All animal protocols were completely approved by the Animal Ethics Committee of Shahid Beheshti University of Medical Sciences and Health Services (Tehran, Iran). First, animals were randomly divided into 5 individual groups (n=8) as follows: (1) defect only (blank control); (2) PTFE/PVA scaffolds; (3) PTFE/PVA/GO scaffolds; (4) PTFE/PVA/Cell (PTFE/PVA scaffolds containing ADSCs); and (5) PTFE/PVA/GO/Cell (PTFE/PVA/GO scaffolds containing ADSCs). All rats were anesthetized with xylazine (5 mg/kg) and methyl-4-hydroxybenzoate (0.3 mg/kg) and skulls were sterilized with povidone-iodine and shaved. The skin and periosteum were slit at the sagittal plane and the skull bone was perforated by dental drill under constant saline irrigation (0.9% NaCl) until an 8 mm bony defect was created while the dura matter was kept intact. Bare scaffolds, PTFE/PVA and PTFE/PVA/GO, and cell-containing scaffolds, PTFE/PVA/Cell and PTFE/PVA/GO/Cell (caring 4×10^6 cells) were incubated in growth medium at 37°C and 5% CO2 since 24 hours prior of implantation. All mentioned scaffolds were implanted while defects at the control group were left without implantation and the skin incision was closed. Randomly selected rats were sacrificed at 6 and 12 weeks after implantation for computerized tomography (CT) analysis and H&E staining (Fig. 1).

CT analysis

At two important time points of bone regeneration (6 and 12 weeks after transplantation), 15 animals (3 animals of each group) were selected randomly and were sacrificed to get examined by the X-ray CT system (InspeXio SMX-90CT; Shimadzu, Kyoto, Japan; resolution, 105 lm;

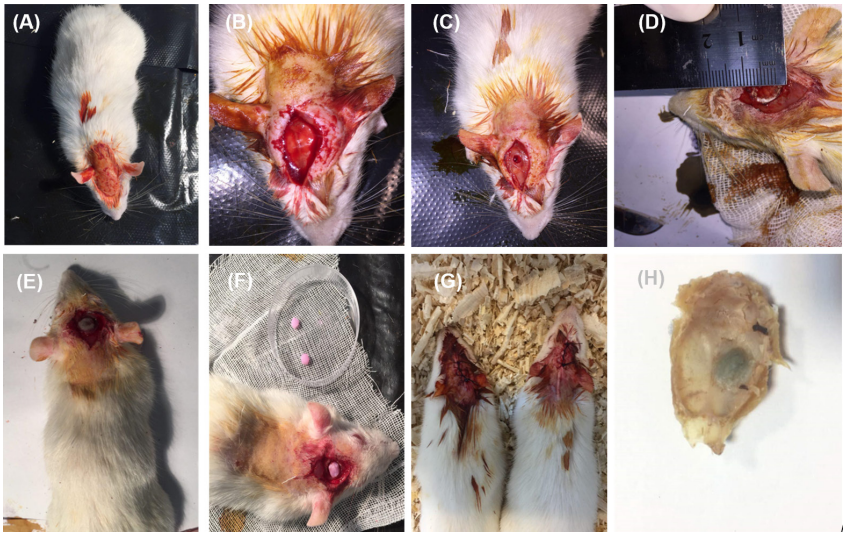

Fig. 1. Surgical procedure. Rat skulls sterilization and shaving (A), skin and periosteum slitting (B), skull bone perforating by dental drill (C), Critical sized calvarial defect (8 mm-diameter) (D), Implanting of bare scaffolds, PTFE/PVA and PTFE/PVA/GO, and cell containing scaffolds, PTFE/PVA/Cell and PTFE/PVA/GO/Cell (E, F), skin incision suturing (G), fixed sample (H).

section-to-section distance, 105 lm) using an InspeXio scanner. Samples were imaged in an arbitrary manner (10 images/each sample) and were analyzed by ImageJ software. Equivalent sites in samples were measured for standardization of analysis.[30]

Histological analysis

To get histological evidence from calvaria after imaging by CT scan, the calvarial bones were removed and prepared for H&E staining taking the following steps: fixing in neutral buffered formalin 10% for 72 hours at room temperature, washing three times with PBS, decalcifying in 10% (w/v) ethylene diamine tetraacetic acid (EDTA) for 3 weeks at 37°C, dehydrating using a graded alcohol series, fixing in 4% paraformaldehyde (Wako, Japan), embedding in paraffin, cutting into 5-µm-thick sections, staining using hematoxylin-eosin (HE; Sigma), and capturing the images.[30]

Results

Scaffolds topography

The scaffolds were completely prepared similar to our previous study.[22] As shown in the scaffolds SEM images in Fig. 2, both scaffolds have multiscale porous and nanofibrous architecture. As we reported before, the porosity of the scaffolds containing graphene oxide nanoparticles was higher (56%) than PTFE/PVA scaffolds (41%). The pores diameter in PTFE/PVA/GO scaffolds (Fig. 2C) were in the range of 800 nm and 750 µm, while the diameters of pores were 417-750 µm in PTFE/PVA scaffolds (Fig. 2A,). Moreover, discontinuous nanofibers with 2-600 nm diameter were expanded into both 3D structures, but the density of the nanofibers was higher in PTFE/PVA/GO scaffolds (Fig. 2D) compared to PTFE/PVA scaffolds (Fig. 2B).

Stem cells characterization

To confirm the expression of mesenchymal stem cells surface markers, flowcytometry analysis was done on ADSCs at the third passage (Fig. 3A). The results showed that ADSCs slightly expressed CD 14, CD20, CD 35, and CD45 (less than 1.29% of the cell population), while significantly expressed CD73, CD90, and CD105 (more than 90% cell population) that were completely compatible with mesenchymal stem cells surface markers profile. As shown in differentiation assay (Fig. 3B, 3C), cultured ADSCs under adipose and osteoinduction medium were successfully differentiated to adipose (Fig.

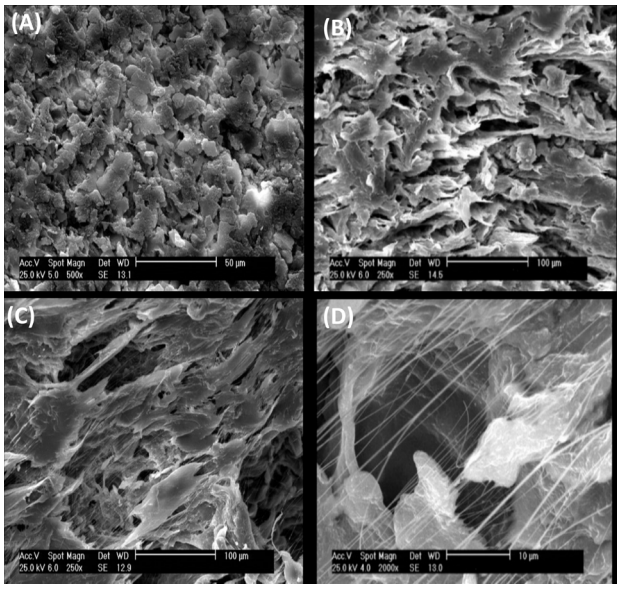

Fig. 2. SEM analysis. Pore and nanofiber topography of PTFE/PVA (A, B, scale bare: 10, 20 µm) and PTFE/PVA/GO scaffolds (C, D, scale bar: 100, 10 µm).

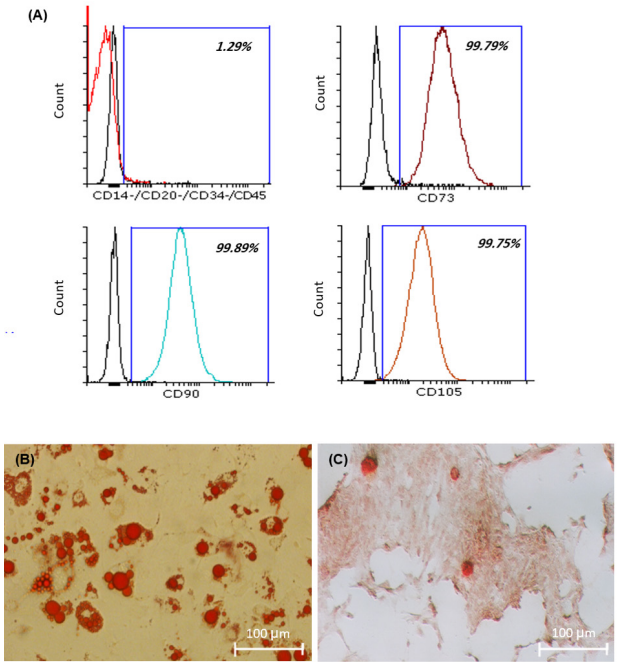

Fig. 3. Flowcytometry analysis (A). ADSCs were slightly expressed CD 14, CD20, CD 35, and CD45, while significantly expressed CD73, CD90, and CD105. Adipose and osteo differentiation assay (B, C). Fat vacuoles inside the cytoplasm of those cells which differentiate to adipose cells stained by oil red O (B, scale bar: 100 µm), Mineralization of those cell which differentiate to osteo visualized by alizarin red S staining (C, scale bar: 100 µm).

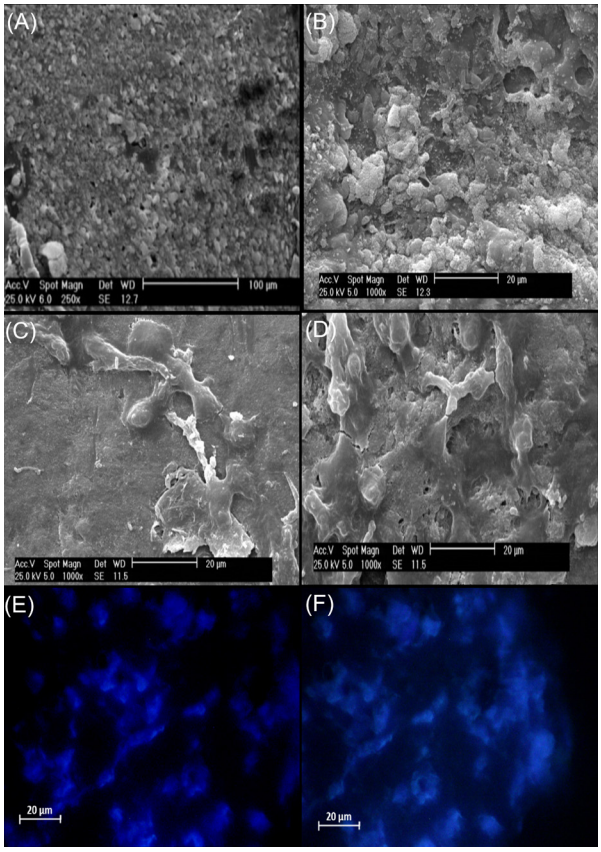

Fig. 4. SEM analysis (A, B, C, D). ADSCs successfully seeded on PTFE/PVA scaffolds (A, C, scale bar: 100, 20 µm) and PTFE/PVA/GO scaffolds (B, D, scale bar: 50, 20 µm) at day 1 (A, B) and 14 (C, D) of culture. DAPI staining (E, F). ADSCs existed on PTFE/PVA (E, scale bar: 20 µm) and PTFE/PVA/GO scaffolds (F, scale bare: 20 µm) at day 7 of cell culture.

3B) and osteogenic cells (Fig. 3C), and their multi linage differentiation capacity was confirmed.

Cell seeding determination

To confirm the quality of cell seeding through the cell culture on scaffolds, SEM analysis at day 1 (Fig. 4A, 4B) and 14 (Fig. 4C, 4D), and DAPI stating at day 7 (Fig. 4E, 4F) were done on randomly selected samples. As shown in Fig. 4, cells were successfully seeded on the scaffolds at two different days of culture.

Osteogenic proteins expression

To confirm the key osteogenic proteins expression through ADSCs seeded on the scaffolds, western blot (Fig. 5) and immunocytochemistry (Fig. 6) were done on days 14 and 21 of culture. As mentioned before, TCPS used as a control for western blot analysis, and nuclei staining with DAPI was used as the control for immunocytochemistry. Fig. 5A shows the related proteins bands including RunX2, Col1α, OCN, and ON in three different groups on days 14 and 21. Semi-quantifying results based on bands image using ImageJ software (Fig. 5B, 5C) showed that the expression of all proteins marker was significantly higher in ADSCs seeded on PTFE/PVA/GO scaffolds compared to ADSCs seeded on PTFE/PVA and TCPS (**P*<0.05). Furthermore, ADSCs seeded on PTFE/PVA showed a higher amount of all protein markers expression compared to TCPS (**P*<0.05). These findings were confirmed by immunocytochemistry results. Fig. 6 (A-X) shows the merged images of the test groups with related control (DAPI staining) showing the expression of all mentioned osteogenic markers at all groups at two different time points (day 14, 21). These images that were semi-quantified using ImageJ software (Fig. 6Y, 6Z) showed that the expression of osteogenic markers was significantly higher in ADSCs seeded on PTFE/PVA/GO scaffolds compared to PTFE/PVA scaffolds.

CT scan analysis

To confirm the quality of the morphology of the defects, CT scan analyses were done at 6 and 12 weeks of implantation. The 2-dimensional defects diameters were measured using CT scan software (Fig. 7 A-H) and the bone healing rate was estimated statistically (Fig. 7I, 7J).[31] Based on the evidence, the defect area diameters at the experimental group implanted by PTFE/PVA/GO scaffolds (Fig. 7B, 7F) were significantly decreased compared to the group implanted by PTFE/PVA scaffolds (Fig. 7A, 7E) at both times points measurements (6, 12 weeks) (**P*<0.005). The healing rate of the defects implanted by the ADSCs containing scaffolds was significantly higher than the group implanted by bare scaffolds at 6 and 12 weeks

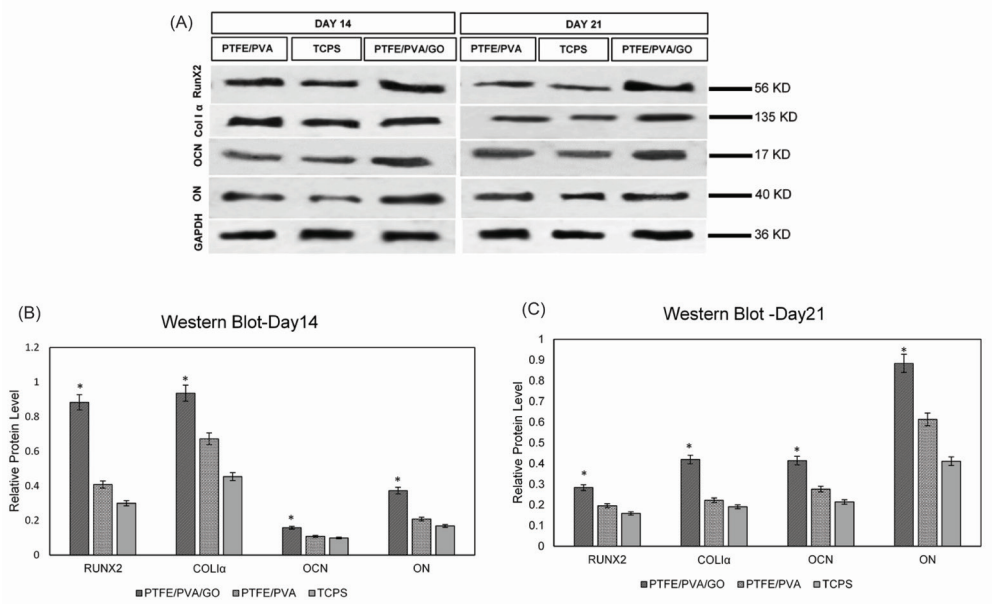

Fig. 5. Western blots of Runx2, Col 1α, ON, OCN at day 14 and 21 of culture (A). Semi-quantifying western blots using ImageJ software (B, C). The results showed that all key osteogenic protein markers were significantly expressed in higher amounts at ADSCs seeded on PTFE/PVA/GO scaffolds compared with ADSCs seeded on PTFE/PVA scaffolds and TCPS (**P*<0.05).

(***P*<0.001, ****P*<0.005). Furthermore, the defects filled by PTFE/PVA/GO/Cell scaffolds at 6 (Fig. 7D) and 12 (Fig. 7H) weeks after implantation showed a higher bone healing rate compared to other groups (****P*<0.005). It should be noted that to enhance the osteogenic potential of hADSCs, the cell containing scaffolds had undergone osteoinduction (OI) for 7 days in vitro.

Hematoxylin & eosin analysis

To investigate new bone-like form development, H&E staining was done at 6 and 12 weeks after implantation. Images of the H&E-stained sections are shown in Fig. 8. Based on the results, there was no sign of new bone-like form tissue in control groups (Fig. 8A, 8B) at 2-time points of investigation. Only finite connective tissue appeared at weeks 6 (Fig. 8A) and 12 (Fig. 8B) in the edge of the defect. On the contrary, a new bone-like form developed from the host bone in all experimental groups (Fig. 8 C-J). Lots of spindle-shaped fibroblast-like cells and a few large round basophilic osteoblast-like cells appeared at week 6 and their number was increased in time in all experimental groups. Based on qualitative images, compared to other groups, the defects filled with PTFE/PVA/GO/Cell scaffolds (Fig. 8I, 8J) showed higher amounts of developing new bone-like tissue and endogenous cell migration from host bone at weeks 6 and 12. Furthermore, new bone-like tissue was developed and expanded more effectively in GO-containing scaffolds (Fig. 8E, 8F, 8I, 8J) compared to other groups.

Discussion

This study aimed to evaluate the potentials of newly designed nanofibrous 3D scaffolds with or without ADSCs for CSCD repair of a rat model. Two types of scaffolds, PTFE/PVA and PTFE/PVA/GO, were synthesized by freeze-drying method as instructed by previously published articles.[22] Scaffolds characterization by SEM confirmed scaffolds multiscale porous and nanofibrous architectures (Fig. 2). The scaffolds' porosity in PTFE/PVA (Fig. 2A) and PTFE/PVA/GO (Fig. 2C) were 41% and 56%, respectively. The pore diameters ranged from 417 to750 µm for PTFE/PVA and 800 nm to 750 µm for PTFE/PVA/GO scaffolds. It was shown that applying GO in scaffold structure increases the average pore size due to its hydrophilic nature. Two main hydrophilic groups in GO structure, -OH and -COOH, provide water absorption sites which ultimately causes more porous structure through ice crystal formation at the freeze-drying process.[32] The nanofiber diameters were 2 to 600 nm in both scaffolds while the fiber density in PTFE/PVA/GO (Fig. 2D) was higher than PTFE/PVA scaffolds (Fig. 2B). These results were attributed to GO unique nano-topography.[33] Many studies investigated the effect of scaffolds topography such as the size of the pores, porosity, fibers density, and orientation, and scaffolds stiffness on stem cells behavior and tissue ingrowth.[34-36] It was shown that the bone-tissue-like ingrowth on different scaffolds needs a range of pore size between 5µm and more than 500 µm. Based on these studies, 100 to 350 µm pores are necessary for bone regeneration while 5 µm and over 500 µm are needed for new functional microvascular networks and rapid vascularization, respectively. Furthermore, pores in the range of 40 to 100 µm influence osteoid ingrowth. Moreover, pore size directly has an impact on the porosity and mechanical properties of scaffolds. Average human bone porosity is 50–90% in trabecular bone and 3–12%

Fig. 6. Immunocytochemistry analysis (A-X, scale bar: 20 µm). Based on the images, expression of RUNX2 by ADSCs at day 14 of culture (A, B, C) was 44.95% at PTFE/PVA (A), 21.9% at TCPS (B), and 64.77% at PTFE/PVA/GO (C) while its expression at day 21 of culture (D, E, F) was 24,54% at PTFE/PVA (D), 19.6% at TCPS (E), and 60.28% at PTFE/PVA/GO (F). Expression of Col 1α by ADSCs at day 14 of culture (G, H, I) was 48.21% at PTFE/PVA (G), 30.46% at TCPS (H), and 63.44% at PTFE/PVA/GO (I) while its expression at day 21 of culture (J, K, L) was 41.7% at PTFE/PVA (J), 25.33% at TCPS (K), and 61.05% at PTFE/PVA/GO (L). Expression of ON by ADSCs at day 14 of culture (M, N, O) was 24.12% at PTFE/PVA (P), 18.4% at TCPS (Q), and 65.9% at PTFE/PVA/GO (R) while its expression at day 21 of culture (P, Q, R) was 49.38% at PTFE/PVA (S), 21.7% at TCPS (T), and 67.8% at PTFE/PVA/GO (U). Expression of OCN by ADSCs at day 14 of culture (S, T, U) was 19.4% at PTFE/PVA (S), 17.85% at TCPS (T), and 51.22% at PTFE/PVA/GO (U) while its expression at day 21 of culture (V, W, X) was 38.4% at PTFE/PVA (S), 19.4% at TCPS (T), and 53.08% at PTFE/PVA/GO (U). Green colour showed detected proteins using specific antibodies, while blue color showed the cells nuclei detected using DAPI staining. Semi-quantifying immunocytochemistry analysis using ImageJ software (Y, Z). The results confirm that the expression of mentioned osteogenic protein markers were significantly higher at ADSCs seeded on PTFE/PVA/GO scaffolds compared with ADSCs seeded on PTFE/PVA scaffolds and TCPS (*P<0.05).

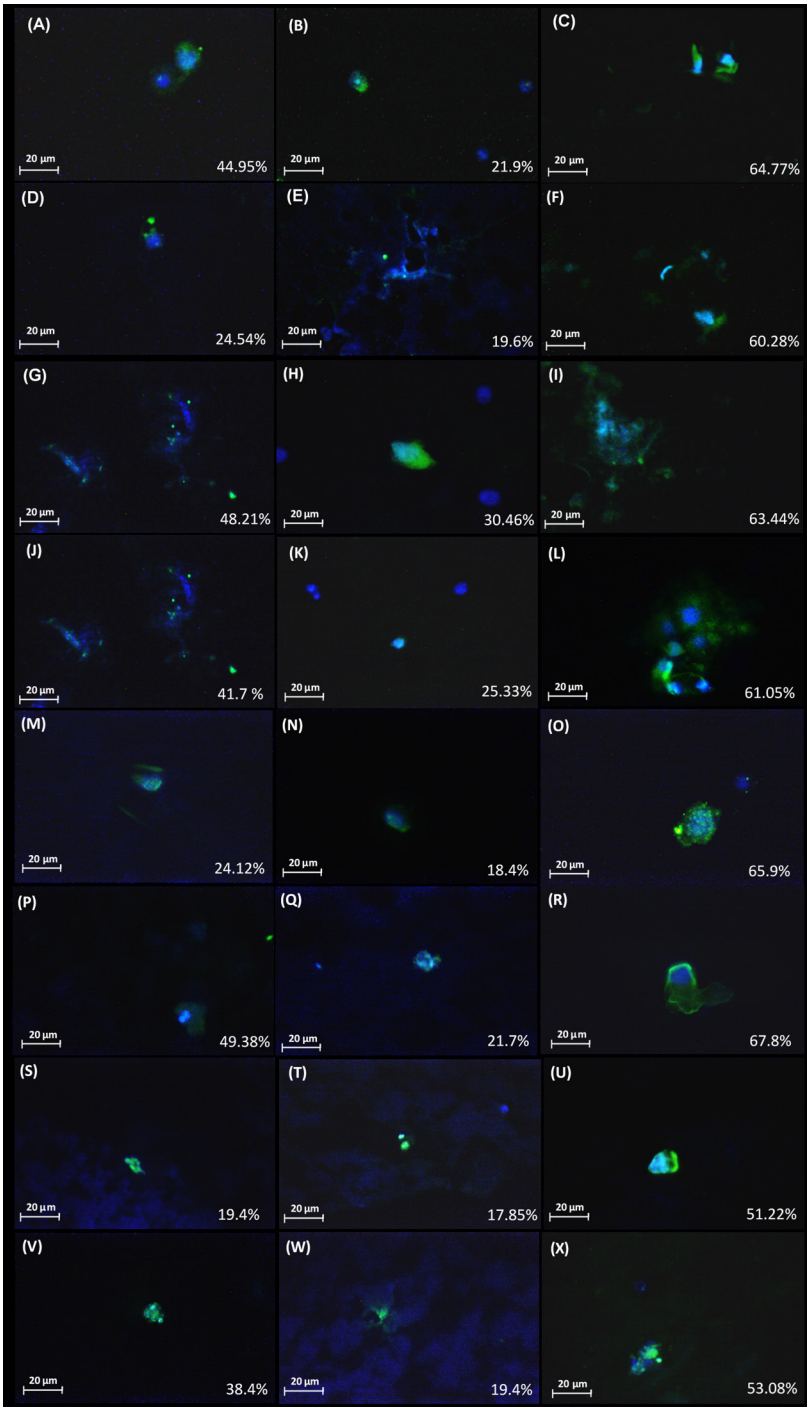

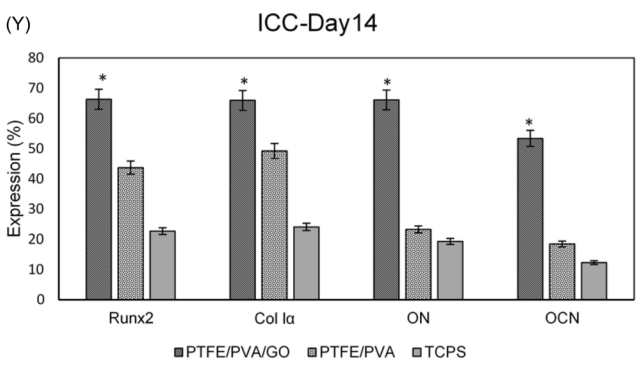

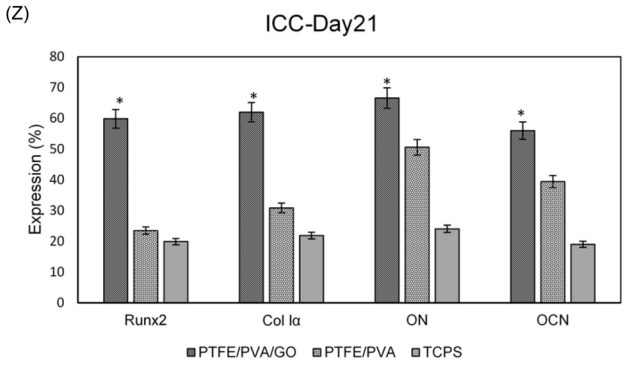

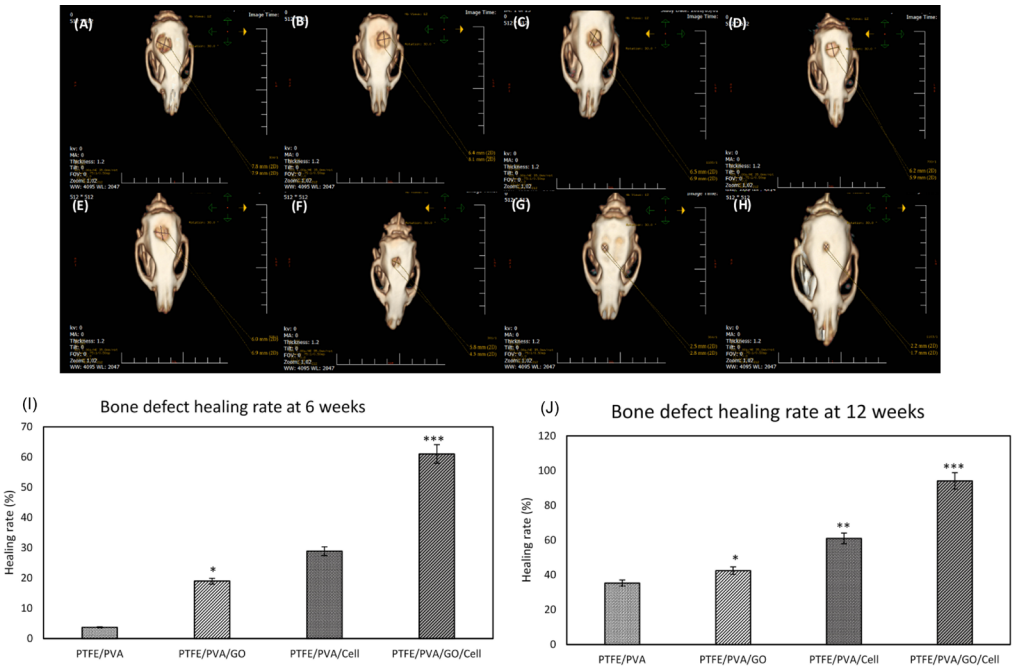

Fig. 7. CT scan images at weeks 6 (Upper row, A, B, C, D) and 12 (lower row, E, F, G, H) after implantation in experimental groups. As shown in the images, the defects dimeter that filled by PTFE/PVA/Cell (C, G) and PTFE/PVA/GO/Cell (D, H) were obviously decreased compared to PTFE/PVA scaffold (A, E) and PTFE/PVA/GO (B, F). Healing rate analysis based on CT scan images at 6 (I) and 12 weeks (J). The results showed that healing rate at defects were filled by GO containing scaffolds were significantly higher than defects were filled by PTFE/PVA at weeks 6 and 12 (** $P < 0.01$). Defects were filled by PTFE/PVA/GO/Cell showed higher healing rate as compared to other groups at weeks 6 and 12 (*** $P < 0.005$). As well as, healing rate at defects were filled by cell containing scaffolds were significantly higher than defects were filled by scaffolds without cells (**$P < 0.05$).

in cortical bone. In literature, there are many successful bone tissue scaffolds with different porosity in the range mentioned above. According to previous findings, besides pore size and porosity, fiber diameter and orientation have an impact on cell attachment, migration, expansion, and differentiation.[37,38] Bone scaffolds need to be able to provide topographical cues of the cell niche, down to 5 nm, to get better cells response.[39] It was reported that stem cell migration on 200-700 nanometer fibers are better than 1.4-4 µm fiber.[8] Also, human mesenchymal stem cells on nanofibers with a diameter less than 400 nanometers are differentiated to osteogenic cell lineage better than on microfiber with a diameter of 1.1-5.7 µm.[8] The natural human bone ECM has the hierarchal structure of aligned tightly packed fibrils proteins that contain mostly collagen type I. This structure provides structural features to control cell attachment, growth, gene expression, migration, and expansion. Recreating the same features in scaffolds will guarantee the scaffolds application outcome.[37] Reduction in fiber diameter and rise in fiber density on GO incorporated scaffolds which was observed in SEM images was consistent with previous reports.[22]

After ensuring the structure of the prepared scaffolds, ADSCs isolated from the human fat pad were cultured in a growth medium. At the third passage, the multi linage differentiation capacity and cell surface markers were detected by Oil Red O (Fig. 3B) and Alizarin S stain (Fig. 3C), as well as flowcytometry (Fig. 3A) The cell samples with spindle morphology were expanded at the bottom of the cell culture flask and successfully differentiated into adipose and osteogenic cells. Moreover, the stem cells significantly expressed CD73, CD90, and CD105 while CD 14, CD20, CD 35, and CD45 expression on the cell surface were less prominent as is expected in mesenchymal stem cells.[25] After cell seeding on two types of scaffolds, the cell existence was detected at the first (Fig. 4A, 4B) and fourteenth day (Fig. 4C, 4D) using SEM, and at the seventh day of culture using DAPI sating (Fig. 4E, 4F). ADSCs on GO-containing scaffolds were higher in number comparing the other group. It might be because of the effect of GO on cell adhesion.[40,41]

In the next step, at days 14 and 21 of culture under osteogenic medium, protein expression of key osteogenic markers including Runx2, COL Iα1, OC, and ON by seeded ADSCs were detected by western blot (Fig. 5) and immunocytochemistry analysis (Fig. 6). Runx2 gene encodes the 56 kD protein that acts as a "master switch" to regulate other genes involved in the development and maintenance of the osteoblast. These genes include alkaline phosphatase, Col Iα1, and OC. They facilitate bone cell phenotype development.[42,43] The results showed that Runx2 protein expression was significantly higher at PTFE/PVA/GO scaffolds compared to PTFE/PVA and TCPS (*$P<0.05$). It might be due to taking the advantage of GO nanoparticle's OH containing groups that facilitate cells attachment and development on the scaffolds. The expression of Runx2 at PTFE/PVA scaffolds

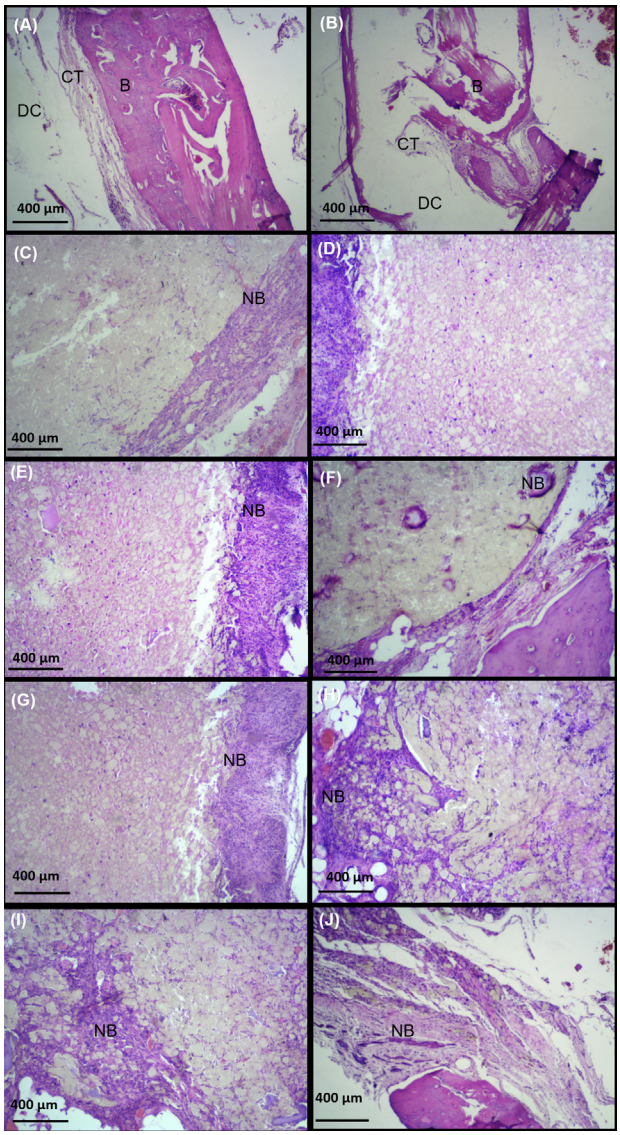

Fig. 8. Hematoxylin eosin staining at 6 (first column, A, C, E, G, K) and 12 (second column, B, D, F, H, L) weeks after implantation (scale bar: 400 µm). The results showed that new bone like tissue (NB) expanded to the scaffolds at defects filled by PTFE/PVA (C, D), PTFE/PVA/GO (E, F), PTFE/PVA/Cell (G, H), and PTFE/PVA/GO/Cell (K, L) as compare to control group (A, B). Host bone (B), Defect cavity (DC), Connective tissue (CT), Osteocyte (OSC), New bon like form tissue (NB).

was higher than TCPS (*$P<0.05$). It might be a result of providing three-dimensional structure for cells in PTFE/PVA scaffolds compared to TCPS. Notably, inconsistent with previous findings, the expression peak of Runx2 was detected on the 14th day of culture and after that day, Runx2 expression started to decrease. Col Iα1, the most abundant ECM protein, organizes the ECM structure and enhances osteogenesis.[44] This protein as an early osteogenic marker was expressed in a higher amount at GO incorporating scaffolds compared to PTFE/PVA and TCPS ($P<0.05$). Similar to Runx2 protein expression, maximum expression of Col Iα1 was detected on the 14th day of culture and then the expression slightly decreased in the rest of the culture days. ON, a secretory glycoprotein has an affinity binding to calcium and collagen. ON has an important role in bone mineralization and facilitates the acquisition of differentiated phenotypes. ON protein expression, as a late osteogenic marker, was detected on the 14th day of culture and then slightly increased during culture. Based on the results, similar to Runx2 and Col Iα1, ON expression were higher on the cells seeded on PTFE/PVA/GO compared to PTFE/PVA and TCPS groups ($P<0.05$) which are attributed to the GO nanoparticles and cells growth on the structure that mimics bone ECM. OCN is secreted only by the osteoblast during the bone formation process. OCN acts as a regulatory protein in the metabolic activity of human cells, bone mineralization, and calcium ion homeostasis. OCN protein is another late osteogenic marker that slightly increased during cell culture in the three mentioned groups. The highest amount was detected on the cells cultured on PTFE/PVA/GO groups ($P<0.05$). The immunocytochemistry assay confirmed all the results acquired by western blot analysis. It is worth mentioning that these findings confirmed our previously published results which were acquired using real-time PCR.[22]

All mentioned proteins were significantly expressed on GO incorporated scaffolds more than other groups (PTFE/PVA and TCPS) ($P<0.05$). Furthermore, the protein expression of Runx2 and COL Iα1 as early osteogenic markers were increased through 14 days of culture. The expression of these markers started to decrease while the protein expression of OC and ON as a late osteogenic marker was slightly increased through 21-day culture under OM. This observation was correlated with GO as a valuable derivation of graphene. It was shown that GO has a tremendous effect on bone regeneration which could be a result of the positive effect of GO on stem cells attachment, growth, expansion, and even differentiation and also on capturing of growth factors from culture media and accumulating them on the scaffold because of its unique nano-topography.[45,46] Furthermore, it was shown that GO affects fiber diameter through fibrous scaffolds fabrication which helps mimic the natural hierarchical bone ECM structure.[36,47]

After confirming the successful osteogenic proteins expression by ADSCs seeded on the two types of scaffolds in the in-vitro study, bare scaffolds and scaffolds with ADSCs were prepared to implant on rat calvarial defects. For this purpose, five groups were defined for implanting: PTFE/PVA and PTFE/PVA/GO with and without ADSCs, as well as a control group with no cells and scaffolds.

Among different types of small and large animals used for BTE including mice, rats, rabbits, dogs, etc rat models are considered the best due to simple and less time taking surgical procedure and exitance of multiple postoperative studies, reproducibility, associate cost, and little morbidity and mortality rate through the study.[48,49] The other important thing is the "critical size defect" term which is accepted as the smallest size of tissue defect that will not

heal without intervention. In rat calvarial defect cases, the 8 millimeters (mm) size is accepted as a critical size defect but many researchers designed their study on the rat models with two 5 mm subcritical sized defects per animal based on their studies objects.[49] In the current study, one 8 mm defect per animal was applied to investigate the bone regeneration potential of the designed constructs. After making defects on the animal's calvarial bone, 4 different types of constructs were implanted and the control group (empty defects) were followed for 6 and 12 weeks. It has been reported that 12 weeks of postoperative follow up is sufficient to estimate bone healing at rodent models. The 4th and 8th weeks after injury, are also critical times in small rodent bone defect healing.[30,49] In this study, 6 and 12 weeks after surgery were chosen to estimate the rate of the healing procedure.

As mentioned above, to compare in-vivo bone formation capabilities of newly designed bare scaffolds (PTFE/PVA, PTFE/PVA/GO) and scaffolds containing ADSCs, they were implanted to the 8 mm circular rat calvarial defects, and the outcomes were evaluated by CT-scan analysis (Fig. 7), and H&E staining (Fig. 8). Blank defects were used as the control group and the experiment were followed at 6 and 12 weeks after implantation. CT images which were captured from the coronal section of the rats' head center between eyes and external acoustic meatus showed that in the groups in which the defects were filled by a cell containing scaffolds (Fig. 7C, 7D, 7G, 7H) finding bone-like tissue was significantly more likely than the groups filled by bare scaffolds (Fig. 7A, 7B, 7E, 7F) ($P<0.05$). This result showed that using ADSCs significantly improves the bone-induced regeneration process when compared to the effect of bare scaffolds. This observation ties well with previous studies wherein culturing ADSCs in scaffolds induces the regeneration of new bone in critical-size defects. It has been demonstrated that it could be a result of pro-osteogenic cytokines secretion by ADSCs in the bone defect areas, osteoblast-like cells derived from ADSCs which produces sufficient osteoid before the maturation of bone by deposition of inorganic salts, and cell-cell interaction between engrafted ASCs and host calvarial osteoblasts which are critical in bony healing of calvarial defects.[50,51] Furthermore, GO-containing scaffolds were more effective than PTEF/PVA scaffolds and showed a dramatic bone defect reduction at two time-point evaluations which are associated with osteoinduction and osteoinductive capabilities of GO nanoparticles. Moreover, histological observation (Fig. 8) showed that bone-like tissue with the typical structure of osteocyte lacunae were formed better in the groups with GO nanoparticles and/or ADSCs while in the controls, the defect sites were mostly filled with fibrous connective tissue. Over time, cells changed their morphology to large round osteoblast-like cells with basophilic cytoplasm and bone ingrowth at the margin of the defect and the central area were observed. There were no wound infections, paralysis, convulsions, or signs of pain during the observation period.

Research Highlights

What is the current knowledge?

√ Freeze drying method could be used for nanofibrous scaffolds production.

What is new here?

√ PTFE/PVA/GO/ADSCs construct has a promising result in in-vivo bone regeneration and could be useful on clinical application.

Conclusion

The data provide evidence that new freeze-dried nanofibrous scaffolds formed from hydrophobic (PTFE) and hydrophilic (PVA) polymers with and without GO make a suitable environment for ADSCs confirmed by the expression of bone-related proteins. Furthermore, bone regeneration at rat calvarial defects were significantly boosted by taking the advantage of ADSCs and GO nanoparticle. PTFE/PVA/GO/ADSCs showed better in-vivo results and is a good candidate for a new cell-scaffold BTE construct for clinical usage.

Acknowledgment

We sincerely acknowledge the School of Advanced Technologies in Medicine and Laser Application in Medical Sciences Research Center, Shahid Beheshti University of Medical Sciences.

Authors' contribution

All authors equally contributed to this study.

Funding sources

No founding sources.

Ethical statement

This study is under the support of Shahid Beheshti University's Medical Research Ethics Committee.

Competing interests

There are no competing interests to declare.

References

1. Chen Y, Xu J, Huang Z, Yu M, Zhang Y, Chen H, et al. An innovative approach for enhancing bone defect healing using PLGA scaffolds seeded with extracorporeal-shock-wave-treated bone marrow mesenchymal stem cells (BMSCs). *Sci Rep* **2017**; 7: 44130. https://doi.org/10.1038/srep44130
2. Roddy E, DeBaun MR, Daoud-Gray A, Yang YP, Gardner MJ. Treatment of critical-sized bone defects: clinical and tissue engineering perspectives. *Eur J Orthop Surg Traumatol* **2018**; 28: 351-362. https://doi.org/10.1007/s00590-017-2063-0
3. Freitas GP, Lopes HB, Souza AT, Oliveira PG, Almeida AL, Souza LE, et al. Cell therapy: effect of locally injected mesenchymal stromal cells derived from bone marrow or adipose tissue on bone regeneration of rat calvarial defects. *Sci Rep* **2019**; 9: 1-13. https://doi.org/10.1038/s41598-019-50067-6
4. Nikolova MP, Chavali MS. Recent advances in biomaterials for 3D scaffolds: A review. *Bioact Mater* **2019**; 4: 271-292. https://doi.org/10.1016/j.bioactmat.2019.10.005

5. Suvarnapathaki S, Wu X, Lantigua D, Nguyen MA, Camci-Unal G. Breathing life into engineered tissues using oxygen-releasing biomaterials. *NPG Asia Mater* **2019**; 11: 1-18. https://doi.org/10.1038/s41427-019-0166-2
6. Caddeo S, Boffito M, Sartori S. Tissue engineering approaches in the design of healthy and pathological in vitro tissue models. *Front Bioeng Biotechnol* **2017**; 5: 40. https://doi.org/10.3389/fbioe.2017.00040
7. Zhu L, Luo D, Liu Y. Effect of the nano/microscale structure of biomaterial scaffolds on bone regeneration. *Int J Oral Sci* **2020**; 12: 1-15. https://doi.org/10.1038/s41368-020-0073-y
8. Jenkins TL, Little D. Synthetic scaffolds for musculoskeletal tissue engineering: cellular responses to fiber parameters. *NPJ Regen Med* **2019**; 4: 1-14. https://doi.org/10.1038/s41536-019-0076-5
9. Holzwarth JM, Ma PX. 3D nanofibrous scaffolds for tissue engineering. *J Mater Chem* **2011**; 21: 10243-10251. https://doi.org/10.1039/C1JM10522A
10. Zhou K, Yu P, Shi X, Ling T, Zeng W, Chen A, et al. Hierarchically porous hydroxyapatite hybrid scaffold incorporated with reduced graphene oxide for rapid bone ingrowth and repair. *ACS Nano* **2019**; 13: 9595-9606. https://doi.org/10.1016/j.biomaterials.2015.01.034
11. Viswanathan P, Ondeck MG, Chirasatitsin S, Ngamkham K, Reilly GC, Engler AJ, et al. 3D surface topology guides stem cell adhesion and differentiation. *Biomaterials* **2015**; 52: 140-147.
12. Chen Z, Ni S, Han S, Crawford R, Lu S, Wei F, et al. Nanoporous microstructures mediate osteogenesis by modulating the osteo-immune response of macrophages. *Nanoscale* **2017**; 9: 706-718. https://doi.org/10.1039/C6NR06421C
13. El-Sherbiny IM, Yacoub MH. Hydrogel scaffolds for tissue engineering: Progress and challenges. *Glob Cardiol Sci Pract* **2013**; 2013: 38. https://doi.org/10.5339/gcsp.2013.38
14. Cascone S, Lamberti G. Hydrogel-based commercial products for biomedical applications: A review. *Int J Pharm* **2020**; 573: 118803. https://doi.org/10.1016/j.ijpharm.2019.118803
15. Caliari SR, Burdick JA. A practical guide to hydrogels for cell culture. *Nat Methods* **2016**; 13: 405-414. https://doi.org/10.1038/nmeth.3839
16. Meng X, Wu T, Qiu D. Toughening anti-overswelling semicrystalline polymer hydrogels with ultra-small hydrophobic nanoparticles. *Polymer* **2020**; 186: 122080. https://doi.org/10.1016/j.polymer.2019.122080
17. Lim J, Lin Q, Xue K, Loh X. Recent advances in supramolecular hydrogels for biomedical applications. *Mater Today Adv* **2019**; 3: 100021. https://doi.org/10.1016/j.mtadv.2019.100021
18. Jiang H, Duan L, Ren X, Gao G. Hydrophobic association hydrogels with excellent mechanical and self-healing properties. *Eur Polym J* **2019**; 112: 660-669. https://doi.org/10.1016/j.eurpolymj.2018.10.031
19. Amruthwar SS, Janorkar AV. In vitro evaluation of elastin-like polypeptide–collagen composite scaffold for bone tissue engineering. *Dent Mater* **2013**; 29: 211-220. https://doi.org/10.1016/j.dental.2012.10.003
20. Nudelman F, Pieterse K, George A, Bomans PH, Friedrich H, Brylka LJ, et al. The role of collagen in bone apatite formation in the presence of hydroxyapatite nucleation inhibitors. *Nat Mater* **2010**; 9: 1004-1009. https://doi.org/10.1038/nmat2875
21. Wang X, Kim HJ, Wong C, Vepari C, Matsumoto A, Kaplan DL. Fibrous proteins and tissue engineering. *Mater Today* **2006**; 9: 44-53. https://doi.org/10.1016/S1369-7021(06)71742-4
22. Khoramgah MS, Ranjbari J, Abbaszadeh H-A, Mirakabad FST, Hatami S, Hosseinzadeh S, et al. Freeze-dried multiscale porous nanofibrous three dimensional scaffolds for bone regenerations. *Bioimpacts* **2020**; 10: 73. https://doi.org/10.34172/bi.2020.10
23. Greenland KN, Carvajal MFCA, Preston JM, Ekblad S, Dean WL, Chiang JY, et al. Order, Disorder, and Temperature-Driven Compaction in a Designed Elastin Protein. *J Phys Chem B* **2018**; 122: 2725-2736. https://doi.org/10.1021/acs.jpcb.7b11596
24. Singla A, Lee CH. Effect of elastin on the calcification rate of collagen-elastin matrix systems. *J Biomed Mater Res* **2002**; 60: 368-374. https://doi.org/10.1002/jbm.10077
25. Abbaszadeh HA, Niknazar S, Darabi S, Ahmady Roozbahany N, Noori-Zadeh A, et al. Stem cell transplantation and functional recovery after spinal cord injury: a systematic review and meta-analysis. *Anat Cell Biol* 2018; 51: 180-188.. https://doi.org/10.5115/acb.2018.51.3.180
26. Jia W, Jiang X, Liu W, Wang L, Zhu B, Zhu H, et al. Effects of three-dimensional collagen scaffolds on the expression profiles and biological functions of glioma cells. *Int J Oncol* **2018**; 52: 1787-1800. https://doi.org/10.3892/ijo.2018.4330
27. Peyvandi AA, Roozbahany NA, Peyvandi H, Abbaszadeh H-A, Majdinasab N, Faridan M, et al. Critical role of SDF-1/CXCR4 signaling pathway in stem cell homing in the deafened rat cochlea after acoustic trauma. *Neural Regen Res* **2018**; 13: 154. https://doi.org/10.4103/1673-5374.224382
28. Fedchenko N, Reifenrath J. Different approaches for interpretation and reporting of immunohistochemistry analysis results in the bone tissue–a review. *Diagn Pathol* **2014**; 9: 1-12. https://doi.org/10.1186/s13000-014-0221-9
29. Abbaszadeh H-A, Tiraihi T, Delshad AR, Zadeh MS, Taheri T. Bone marrow stromal cell transdifferentiation into oligodendrocyte-like cells using triiodothyronine as a inducer with expression of platelet-derived growth factor α as a maturity marker. *Iran Biomed J* **2013**; 17: 62. https://doi.org/10.6091/ibj.11162.2013
30. Spicer PP, Kretlow JD, Young S, Jansen JA, Kasper FK, Mikos AG. Evaluation of bone regeneration using the rat critical size calvarial defect. *Nat Protoc* **2012**; 7: 1918-1929. https://doi.org/10.1038/nprot.2012.113
31. Cukjati D, Reberšek S, Miklavčič D. A reliable method of determining wound healing rate. *Med Biol Eng Comput* **2001**; 39: 263-271. https://doi.org/10.1007/BF02344811
32. Sivashankari P, Prabaharan M. Three-dimensional porous scaffolds based on agarose/chitosan/graphene oxide composite for tissue engineering. *Int J Biol Macromol* **2020**; 146: 222-231. https://doi.org/10.1016/j.ijbiomac.2019.12.219
33. Qi Y, Tai Z, Sun D, Chen J, Ma H, Yan X, et al. Fabrication and characterization of poly (vinyl alcohol)/graphene oxide nanofibrous biocomposite scaffolds. *J Appl Polym Sci* **2013**; 127: 1885-1894. https://doi.org/10.1002/APP.37924
34. Chen X, Fan H, Deng X, Wu L, Yi T, Gu L, et al. Scaffold structural microenvironmental cues to guide tissue regeneration in bone tissue applications. *Nanomaterials* **2018**; 8: 960. https://doi.org/10.3390/nano8110960
35. Henkel J, Woodruff MA, Epari DR, Steck R, Glatt V, Dickinson IC, et al. Bone regeneration based on tissue engineering conceptions—a 21st century perspective. *Bone Res* **2013**; 1: 216-248. https://doi.org/10.4248/BR201303002
36. Bhattarai DP, Aguilar LE, Park CH, Kim CS. A review on properties of natural and synthetic based electrospun fibrous materials for bone tissue engineering. *Membranes* **2018**; 8: 62. https://doi.org/10.3390/membranes8030062
37. Cun X, Hosta-Rigau L. Topography: A Biophysical Approach to Direct the Fate of Mesenchymal Stem Cells in Tissue Engineering Applications. *Nanomaterials* **2020**; 10: 2070. https://doi.org/10.3390/nano10102070
38. Murphy CM, Haugh MG, O'brien FJ. The effect of mean pore size on cell attachment, proliferation and migration in collagen–glycosaminoglycan scaffolds for bone tissue engineering. *Biomaterials* **2010**; 31: 461-466. https://doi.org/10.1016/j.biomaterials.2009.09.063
39. Metavarayuth K, Sitasuwan P, Zhao X, Lin Y, Wang Q. Influence of surface topographical cues on the differentiation of mesenchymal stem cells in vitro. *ACS Biomater Sci Eng* **2016**; 2: 142-151. https://doi.org/10.1021/acsbiomaterials.5b00377
40. Lee WC, Loh KP, Lim CT. When stem cells meet graphene: Opportunities and challenges in regenerative medicine. *Biomaterials* **2018**; 155: 236-250. https://doi.org/10.1016/j.

biomaterials.2017.10.004
41. Halim A, Luo Q, Ju Y, Song G. A mini review focused on the recent applications of graphene oxide in stem cell growth and differentiation. *Nanomaterials* **2018**; 8: 736. https://doi.org/10.3390/nano8090736
42. Pratap J, Galindo M, Zaidi SK, Vradii D, Bhat BM, Robinson JA, et al. Cell growth regulatory role of Runx2 during proliferative expansion of preosteoblasts. *Cancer Res* **2003**; 63: 5357-5362.
43. Komori T. Regulation of proliferation, differentiation and functions of osteoblasts by Runx2. *Int J Mol Sci* **2019**; 20: 1694. https://doi.org/10.3390/ijms20071694
44. Lin X, Patil S, Gao Y-G, Qian A. The bone extracellular matrix in bone formation and regeneration. *Front Pharmacol* **2020**; 11: 757. https://doi.org/10.3389/fphar.2020.00757
45. Prasadh S, Suresh S, Wong R. Osteogenic potential of graphene in bone tissue engineering scaffolds. *Materials* **2018**; 11: 1430. https://doi.org/10.3390/ma11081430
46. Li M, Xiong P, Yan F, Li S, Ren C, Yin Z, et al. An overview of graphene-based hydroxyapatite composites for orthopedic applications. *Bioact Mater* **2018**; 3: 1-18. https://doi.org/10.1016/j.bioactmat.2018.01.001
47. Wang B, Cai Q, Zhang S, Yang X, Deng X. The effect of poly (L-lactic acid) nanofiber orientation on osteogenic responses of human osteoblast-like MG63 cells. *J Mech Behav Biomed Mater* **2011**; 4: 600-609. https://doi.org/10.1016/j.jmbbm.2011.01.008
48. McGovern JA, Griffin M, Hutmacher DW. Animal models for bone tissue engineering and modelling disease. *Dis Model Mech* **2018**; 11: dmm033084. https://doi.org/10.1242/dmm.033084
49. Gomes P, Fernandes M. Rodent models in bone-related research: the relevance of calvarial defects in the assessment of bone regeneration strategies. *Lab Anim* **2011**; 45: 14-24. https://doi.org/10.1258/la.2010.010085
50. Levi B, Longaker MT. Concise review: adipose-derived stromal cells for skeletal regenerative medicine. *Stem Cells* **2011**; 29: 576-582. https://doi.org/10.1002/stem.612
51. Gao S, Calcagni M, Welti M, Hemmi S, Hild N, Stark WJ, et al. Proliferation of ASC-derived endothelial cells in a 3D electrospun mesh: Impact of bone-biomimetic nanocomposite and co-culture with ASC-derived osteoblasts. *Injury* **2014**; 45: 974-980. https://doi.org/10.1016/j.injury.2014.02.035